PNAS
www.pnas.org

Supplementary Information for

Growth Model Interpretation of Planet Size Distribution

Authors: Li Zeng*[1,2], Stein B. Jacobsen[1], Dimitar D. Sasselov[2], Michail I. Petaev[1,2], Andrew Vanderburg[3], Mercedes Lopez-Morales[2], Juan Perez-Mercader[1], Thomas R. Mattsson[4], Gongjie Li[5], Matthew Z. Heising[2], Aldo S. Bonomo[6], Mario Damasso[6], Travis A. Berger[7], Hao Cao[1], Amit Levi[2], Robin D. Wordsworth[1].

*Correspondence to: astrozeng@gmail.com

This PDF file includes:

Materials and Methods
Figure S1
Figure S2
Table S1
References for SI reference citations

Materials and Methods

Planet data of all exoplanets used for our analysis have been downloaded from the *NASA Exoplanet Archive* (*1*, *2*) on several occasions, with the manual addition/modification of some newly-discovered planets: in particular, on Nov.10, 2016 for initial mass-radius plot and statistical assessments, and subsequently on Feb.10, May 31, Sept.9, Oct.16, 2017, and Feb.20, Jun.15, 2018 for updates. Moreover, we have updated the radii of some planets below 8 $R_\oplus$ with GAIA DR1 (*3*) and GAIA DR2 (*4*). To make the mass-radius plot more precise, we select planets with density constraints better than about ±50%.
Specifically, since density $\rho \propto M/R^3$, taking natural logarithmic gives $\ln \rho = \ln M - 3 \ln R + const$, and differentiation of it gives: $\frac{d\rho}{\rho} = \frac{dM}{M} - 3 \cdot \frac{dR}{R}$.
Error propagation assumes errors of mass and radius are independent: $\frac{\sigma\rho}{\rho} \approx \sqrt{\left(\frac{\sigma M}{M}\right)^2 + \left(3 \cdot \frac{\sigma R}{R}\right)^2}$
Then, taking into account asymmetric error bars to avoid planets with an extremely large error bar in one direction, we chose the selection criterion as:

$$\ln\left(\frac{\rho + \sigma\rho^+}{\rho - \sigma\rho^-}\right) \approx \sqrt{\left[\ln\left(\frac{M + \sigma M^+}{M - \sigma M^-}\right)\right]^2 + \left[3 \cdot \ln\left(\frac{R + \sigma R^+}{R - \sigma R^-}\right)\right]^2} \lesssim 1$$

where the + and – signs denote the error bar in the plus and minus direction respectively. The planet data are listed in (**SI Appendix, Table S1**), with detailed references (*3–80*).

Figs. 1, 2, & 4 have been plotted using this selection criterion with the built-in schemes in *Mathematica (Version 11)* including "ListLogLogPlot" and "ErrorListPlot".

Statistical analysis of the planet data has been performed with *Mathematica*'s built-in "WeightedData", "SmoothHistogram", and "SmoothKernelDistribution" packages. The smoothing is done with the *Mathematica*'s default "Silverman" bandwidth-selection-method. Each planet data is weighted by the product of its positive and negative 1-σ mass error bars. We then calculate the weighted mean and weighted standard deviation for each set of planets.

Observations bias of the RV method tends to detect and characterize planets of higher masses and orbiting closer to their host stars (*81*). Because of this bias, the RV method becomes more sensitive as mass of a planet increases at given orbit, with current detection limit of ~3 $M_\oplus$. When we invert the RV mass distribution to a radius distribution, we miss the planets smaller than ~1.4 $R_\oplus$. Because such planets are not taken into account by our simulations, our Monte Carlo histogram (gray bars in **Fig. 2**) has much less planets below ~1.4 $R_\oplus$ than observed by the transiting method. This also results in a slightly higher radius gap compared to the population detected by the transiting method. Since this paper considers planets more massive than ~3 $M_\oplus$, the observational bias of the RV method has little effect on our results and conclusions.

Multi-planet systems which contain both super-Earths and sub-Neptunes are interesting. First of all, the goal of our paper is not to model a specific exoplanetary system but rather to use the observed statistical distributions for identifying possible nature of different planet populations. This is why we focus on the majority of exoplanets found by the *Kepler* mission. Our growth model is statistical in nature and does not intend to explain detailed architecture of a specific planetary system. Such outliers and extreme cases constitute ~5% of the observed exoplanet population which our model cannot explain. Indeed, real planet-forming scenarios are more complicated and, perhaps, somewhat different around different stars. One of the critical features in different disks would be how and when the snowlines and planet-building materials migrate during planet formation. For example, taking into account formation of a planet at a snowline followed by its inward migration, Ormel et al. 2017 (*82*) managed to explain the formation and architecture of compact multi-planet systems such as *Trappist*-1 (*70*, *76*, *83*). *Kepler*-20 (*26*, *84*, *85*) can be also explained by such scenario. We call this scenario the "snowline conveyor belt hypothesis" which is consistent with our growth model. In addition, planet-planet collisions (i.e. giant impacts), and more generally, strong dynamical interactions among planets during planet formation have long been suggested by planet formation theory, and recently have been confirmed by the observation and characterization of the *Kepler*-107 system (*86*, *87*).

TTV planets. The mass determination from transit-timing-variation (TTV) for multi-planet systems is known to be difficult and, often requires a later revision, because the masses determined are often degenerate with the combined eccentricities of planets in that system (*88*). Sometimes the N-body Markov-Chain-Monte-Carlo (MCMC) approach is used to find the best solutions. When a longer time duration of TTV observations becomes available, or data are re-assessed by a different group, the planet masses can change significantly; e.g., *Trappist*-1 system (*70*, *83*, *89*, *90*) and *Kepler*-11 system (*68*, *71*, *72*). Some TTV planets (**Fig. 2**) of 2-4 $R_\oplus$ seem to be puffy, i.e., of low-bulk-density. They can be explained by a core (rocky/icy, 3-10 $M_\oplus$) plus a thick, but very light (1~2% of total planet mass) gaseous envelope. Also, statistically speaking, systems with significant TTV effects are less common among all *Kepler* planetary systems; e.g., among 2599 *Kepler* Objects of Interest (KOIs) only 260 were found with significant TTVs with long-term (>100 day) variations (*67*). TTV systems are generally characterized by tight spacing of planets, circular (low $\boldsymbol{e}$) and coplanar (low $\boldsymbol{i}$) orbits, and low obliquities of the host stars (*91*). The difference in planet masses between TTV and RV may be correlated with the host stellar metallicities – TTV planets prefer low-metallicity host stars (*92*). They can be explained by planet formation under different disk conditions, e.g., solid surface density versus gas surface density in the disk (*93*, *94*).

Transitional planets (of 4-10 $R_\oplus$), in particular the ones slightly larger than 4 $R_\oplus$ residing to the right of the purple growth curves in **Fig. 1**, have massive cores ($\gtrsim$20 $M_\oplus$) but not much gas ($\lesssim$20% by mass). For example, K2-55 b (stellar [Fe/H]=0.376±0.095) has core mass estimated to be ~40 $M_\oplus$ with about 10% H_2/He envelope by mass, regardless of the core composition (rocky or icy) (*95*). Because their core masses are apparently above the critical core mass (*96*–*98*), it is interesting to understand how they could have formed with that much solid material without experiencing a runaway gas accretion. One hypothesis is that they arise as mergers of two or more less massive cores. The merging processes tend to merge the denser cores together but (partially) erode their gas envelopes (*99*, *100*), resulting in a net mass increase accompanied by a very small radius increase, that moves them to the right on the mass-radius diagram. Disks with high metallicity may facilitate mergers. The second hypothesis is motivated by the results of micro-lensing surveys (*101*, *102*), which are sensitive to distant planet populations orbiting their host stars typically at a few a.u. The results show that planets in the 20-80 $M_\oplus$ range at a few a.u. are abundant, which is contradictory to the paucity of planets of this mass range predicted by runaway gas accretion models. This suggests that the current runaway core accretion models may require significant revisions to slow down the growth of planets of 10-50 $M_\oplus$ and start the runaway accretion at higher masses of 50-80 $M_\oplus$ instead of 10 $M_\oplus$. The third hypothesis assumes that part of planet formation takes place when the gas in the disk is depleted; cf. theoretical calculations of transitional disks (*103*) and the inferred rapid gas depletion by a few million years from the ALMA survey of the Lupus Proto-planetary disks (*104*, *105*). However, one has to be cautious that the distinction between the total gas depletion and CO depletion cannot be inferred from observation directly, because the inferred H_2 depletion is calculated based on the observed CO depletion and assumed ISM-like [CO]/[H_2] ratio (per. comm. Jane Huang and Sean

Andrews). The cores of these transitional planets, regardless of a hypothesis of their origin, likely contain large fractions of ices in addition to rocks, just as Uranus and Neptune.

Mass-radius curves. The mass-radius curves (**Figs. 1 & 2**) allow calculations of average densities and further constraining the planet bulk compositions and internal structures following the methods that we published earlier (*106–109*) and similar efforts from other researchers in our field (*110–120*). The H_2-He is assumed to be a cosmic mixture of 75% H_2 and 25% He by mass (*121–123*). The Earth-like composition is assumed to be 32.5 wt.% Fe/Ni-metal plus 67.5 wt.% $MgSiO_3$-rock. The bulk H_2O in deep interior is assumed to be in solid phase along the melting curve (liquid-solid phase boundary) (*124–131*). The colored H_2O M-R curves correspond to isothermal vapor/liquid/super-critical fluid envelope at various surface temperatures: 300K, 500 K, 700 K, and 1000 K, on top of ice VII-layer along the appropriate melting pressure (*132–134*). Since ices all have similar densities, and the H_2O-NH_3-CH_4 mixture is always dominated by H_2O due to chemistry evaluation, the mass-radius curve of the H_2O-NH_3-CH_4 mixture is expected to be very similar to that of pure-H_2O. On the other hand, the H_2-He mass-radius curves are calculated along various interior adiabats at different internal specific entropies, labelled by the temperature of the corresponding specific entropy at 100-bar level in the gas envelope (400K, 1000K, 3000K). The mass-radius curves are almost parallel to one another and do not criss-cross, as in all cases at high pressure the material structure is supported mainly by the electron degeneracy pressure, which has similar functional dependence on compression. Therefore, the density of a particular material under high pressure is primarily determined by its average atomic weight, which is very different for the three major planet-building materials: rocks, ices, H_2-He gas, resulting in significant density differences among them in planetary deep interiors, and secondarily by the crystal structure or temperature. The surface of a planet in our calculation is always defined at 10^-3 bar (1 milli-bar) level as an approximate for the level that transiting observations probe.

H_2O EOS. The **equations of states (EOS)** of ice and ice-mixtures under appropriate pressure and temperature conditions are required to understand the interiors of these water worlds. Density Functional Theory calculations based on quantum mechanics have provided thermo-physical properties of water at extreme conditions, including predictions of superionic phases (*127*, *129*). Importantly, key results from DFT simulations have been validated by experiments on Sandia's Z-machine (*135*) as well as by direct measurements of proton conductivity in diamond anvil cell experiments (*136*) and shock compression experiments (*128*). Various models of planet interiors utilizing those EOSs have been introduced (*137*). These models make predictions of the existence of intriguing phases such as the super-ionic state of hot ices and also the non-dipole magnetic field generated in the interior of such planets. They also show that H_2O EOS commonly used in some previous planetary models significantly overestimate the compressibility, and consequently overestimate the density of water at a few hundred GPa (*135*), relevant to the interior of these intermediate-sized planets. This new water EOS (*135*) is adopted for our calculation.

Growth curves. The growth curves of either adding H_2O-ice (cyan) or H_2-He gas (purple) to a core are calculated (**Figs. 1 & 2**). The cyan growth curves start with 4 and 8 $M_\oplus$ rocky cores and show the trajectory of a growing planet on the mass-radius diagram with increasing amount of H_2O added. The purple growth curves start with 8 and 16 $M_\oplus$ icy cores (half-ice and half-rock by mass) and show the trajectory of a growing planet on the mass-radius diagram with increasing amount of cold H_2-He gas added. The tangential slope of the growth curve on the mass-radius diagram depends on the ratio between the density of the added material versus the density of the already-existing material on the planet. The initial slope of a growth curve on a log-log mass-radius plot can be approximated as $d\ln R/d\ln M \sim \rho_{core}/(3\rho_{acc})$, where ρ_{core} is the core density and

ρ_{acc} is the density of added material. The tangential slope of the growth curve of H_2-He is nearly vertical initially, due to the very low density of gas, regardless of the core composition---rocky or icy. The H_2-He gaseous envelope of 1-2 $R_\oplus$ thick is insignificant in mass---a few percent in mass% (*138*, *139*). Until more and more H_2-He is added so that the H_2-He in the planetary deep interiors become self-compressed to high enough densities, so that the tangential slope of H_2-He growth curve reduces. A *Mathematica* program for this calculation is available upon request. However, be cautious that a simple growth curve is not to be understood as a realistic time-evolution for a single planet growth, such that a planet core must accrete all rocks before accreting any ices. But rather, it is a statistical trend followed by comparing the overall planet populations. In fact, it is more likely that the earlier condensed dust in the nebula is entrapped into multi-layers of ices---icy pebbles (**SI Appendix, Fig. S1**). Then, a planet core, if formed beyond or near the snowline, or if accreting icy pebbles, would accrete rocks and ices simultaneously. The dichotomy of rocky versus icy bodies is also reflected in the densities of solar system giant planets' satellites (**SI Appendix, Fig. S2**).

Monte Carlo simulation. We conduct a series of Monte Carlo simulations, in order to test our model of rocky and intermediate-sized planetary mass-radius relation, which provide clues on the composition of the planets. Specifically, we first sample the planetary masses using the observed mass distribution, where the masses of the rocky worlds are generated following the empirical smooth kernel distribution of planets with radii between 1.4-1.9 $R_\oplus$, and the masses of the icy worlds follow the empirical smooth kernel distribution of those with radii between 2-3 $R_\oplus$. Then, we calculate the radii of the planets based on the mass-radius relation: the radii of the rocky worlds can be obtained equating $R=M^{1/3.7}$ (*108*, *140*), and the radii of the intermediate-sized worlds can be calculated as $R=f\times M^{1/3.7}$. f is an indicator of the composition of the intermediate-sized planet. For instance, f=1, if the intermediate-sized worlds still follow the rocky planetary mass-radius relation. f=(1+0.55 x-0.14 x^2), where the ice mass fraction "x" of the icy world is around 1/2~2/3, depending on incorporating the more volatile (C,N)-clathrate-ices or not. For a complete water world (100% water), f=1.41. In order to compare with the observed exoplanets with RV mass measurements, we assume that "x" follows a uniform distribution in between 1/2 and 2/3 for the icy worlds, corresponding to fully incorporating H_2O ices in proportion to rocks, and partially incorporating (C,N)-clathrate-ices in some cases. Then we include an additional ±7% uncertainty to account for the observational errors in planetary radii, and an additional ±30% uncertainty to account for the observational errors in planetary masses. Combining the Monte Carlo results of these two populations and adopt a number ratio of #rocky cores : #icy cores = 1 : 2, we recover the bimodality with the planet radius gap matches the observation in the mass-radius diagram (**Fig. 2**). The generated 2-dimensional mass-radius histogram and the 1-dimensional radius histogram are only meant to be compared with the observed planet populations in between 1.4-3 $R_\oplus$, since our assumption in generating this Monte Carlo simulation draws the empirical mass distribution only from within this radius range. Therefore, planets larger than about 3 $R_\oplus$ generally require the presence of some gaseous envelope, and this is beyond the scope of this simulation. This gas envelope could either be primordial H_2-He-dominated nebular gas or could be formed by the dissociation and vaporization of the ices near the surface and in the atmosphere of these planets. This **Monte Carlo** simulation is performed using *Mathematica*'s built-in random number generator "RandomVariate". "DensityHistogram" is used for the 2-dimensional plot of the probability density contours from the Monte Carlo simulation results. A *Mathematica* program for generating the Monte Carlo simulation is available upon request.

Supplementary Figures:

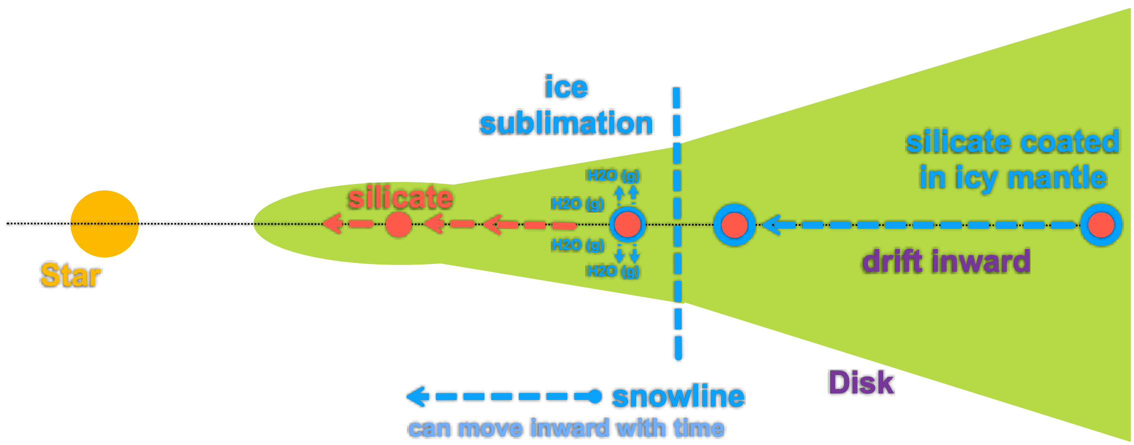

Fig. S1 Cartoon of a protoplanetary disk showing the inward drift of solid particles consisting of silicates (red) and ices (blue). When particles cross the snowline (vertical blue dashed line) they start losing ice by sublimation. Larger particles of pebble size may drift deeper into the inner zone until they completely loose ice. The snowline itself would move inward as the disk cools with time (*141–143*). Large icy planetary cores formed beyond snowline can later migrate inward due to planet-disk interactions (*144–146*) or planet-planet scattering (*147*).

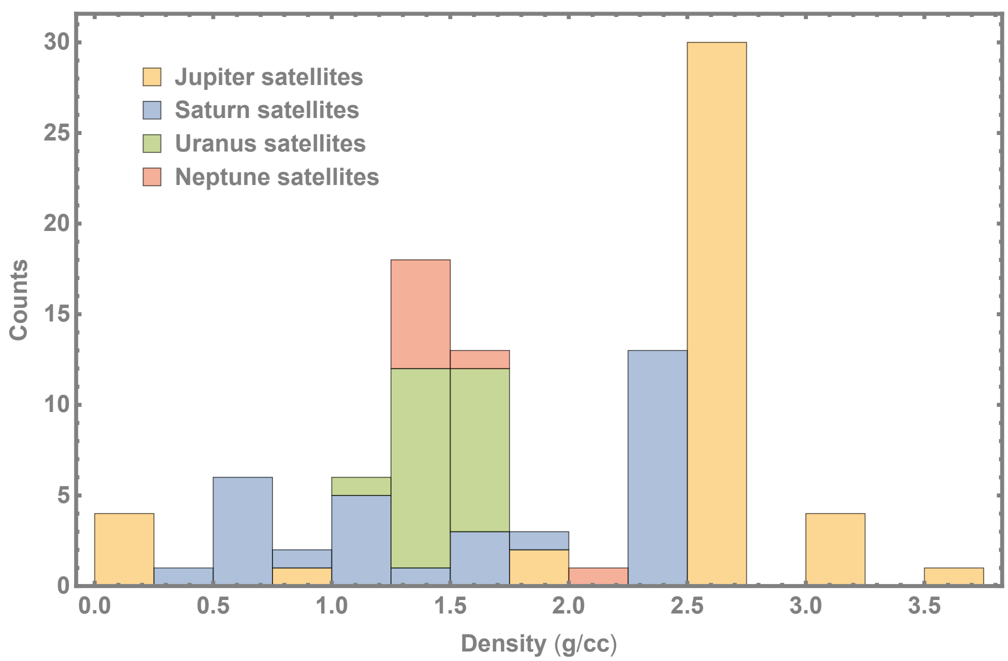

Fig. S2 Density variations among satellites of the outer Solar System planets. The two well-defined peaks at ~1.5 and ~2.5 g/cc suggest that the planet formation process involved interactions between both icy and rocky bodies.

Table S1.

<u>ref.</u> (*3*–*80*).
This file is modified from the NASA Exoplanet Archive (*1*, *2*): http://exoplanetarchive.ipac.caltech.edu
COLUMN pl_orbper: Orbital Period [days]
COLUMN pl_ttvflag: TTV Flag (1=yes, 0=no)
COLUMN st_teff: Host Stellar Effective Temperature [K]
COLUMN st_mass: Host Stellar Mass [Solar mass = 1.9885 * 10^30 kg]
COLUMN st_rad: Host Stellar Radius [Solar radii = 6.957 * 10^8 meter]
COLUMN pl_name: Planet Name
COLUMN pl_rvflag: Planet RV Flag (1=yes, 0=no)
COLUMN pl_masse: Planet Mass [Earth mass = 5.972 * 10^24 kg]
COLUMN pl_masseerr1: Planet Mass Upper Unc. [Earth mass]
COLUMN pl_masseerr2: Planet Mass Lower Unc. [Earth mass]
COLUMN pl_rade: Planet Radius [Earth radii = 6.371 * 10^6 meter]
COLUMN pl_radeerr1: Planet Radius Upper Unc. [Earth radii]
COLUMN pl_radeerr2: Planet Radius Lower Unc. [Earth radii]
COLUMN met: Host Stellar Metallicity [Fe/H]
COLUMN mass_ref: Reference to the Planet Mass adopted
COLUMN radius_ref: Reference to the Planet Radius adopted
COLUMN additional_ref: Additional Reference
#

#	pl_orbper	pl_ttvflag	st_teff	st_mass	st_rad	pl_name	pl_rvflag	pl_masse	pl_masseerr1	pl_masseerr2	pl_rade	pl_radeerr1	pl_radeerr2	met	mass_ref	radius_ref	add_ref
RV planets < 1.4 Earth radii																	
1	0.584249	0	5185	0.837	0.793	K2-229 b	1	2.59	0.43	-0.43	1.164	0.066	-0.048	-0.09	Santerne_2018	Santerne_2018	
2	1.6289287	0	3270	0.181	0.211	GJ 1132 b	1	1.66	0.23	-0.23	1.13	0.056	-0.056	null	Bonfils_2018	Dittman_2017	Diamond-Lowe_2018
3	0.355007	0	5058	0.76	0.74	K-78 b	1	1.87	0.27	-0.26	1.2	0.09	-0.09	-0.14	Grunblatt_2015	Grunblatt_2015	
4	3.777931	0	3216	0.179	0.2139	LHS 1140 c	1	1.81	0.39	-0.39	1.282	0.024	-0.024	-0.24	Ment_2018	Ment_2018	Dittmann_2017

RV planets 1.4-2.0 Earth radii

1	2.17	0	4503	0.7	0.72	K2-216 b	1	7.4	2.2	-2.2	1.8	0.2	-0.1	-0.18	Persson_2018	Persson_2018	Mayo_2018
2	0.7365	0	5172	0.91	0.94	55 Cnc e	1	8	0.3	-0.3	1.88	0.03	-0.03	0.31	Demory_2016	Bourrier_2018	Winn_2011
3	0.8536	0	5259	0.91	0.82	CoRoT-7 b	1	5.74	0.86	-0.86	1.7	0.1	-0.1	0.05	Barros_2014	Stassun_2017	Haywood_2014
4	3.0929	0	4699	0.81	0.78	HD 219134 b	1	4.74	0.19	-0.19	1.602	0.055	-0.055	0.11	Gillon_2017	Gillon_2017	Motalebi_2015
5	6.7646	0	4699	0.81	0.78	HD 219134 c	1	4.36	0.22	-0.22	1.511	0.047	-0.047	0.11	Gillon_2017	Gillon_2017	Motalebi_2015
6	0.9596	0	5261	0.86	0.86	HD 3167 b	1	5.02	0.38	-0.38	1.7	0.18	-0.15	0.04	Christiansen_2017	Christiansen_2017	Gandolfi_2017
7	24.64	0	3896	0.6	0.56	K2-3 c	1	3.1	1.3	-1.2	1.77	0.18	-0.18	-0.01	Damasso_2018	Damasso_2018	Sinukoff_2016
8	44.56	0	3896	0.6	0.56	K2-3 d	1	2.7	1.2	-0.8	1.65	0.17	-0.17	-0.01	Damasso_2018	Damasso_2018	Sinukoff_2016
9	0.5713	0	5470	0.945	0.87	K2-106 b	1	8.36	0.96	-0.94	1.52	0.16	-0.16	-0.025	Guenther_2017	Guenther_2017	Sinukoff_2017 Adams_2017
10	0.3693	0	5200	0.84	0.81	K2-131 b	1	6.5	1.6	-1.6	1.81	0.16	-0.12	0	Dai_2017	Dai_2017	Mayo_2018
11	0.2803	0	4599	0.71	0.68	K2-141 b	1	5.08	0.41	-0.41	1.51	0.05	-0.05	-0.06	Malavolta_2018	Malavolta_2018	Barragan_2018
12	0.8375	0	5599	0.91	1.09	K-10 b	1	4.61	1.27	-1.46	1.489	0.07	-0.062	-0.15	Esteves_2015	Berger_2018	Dumusque_2014
13	3.6961	0	5508	0.95	0.89	K-20 b	1	9.7	1.41	-1.44	1.707	0.08	-0.068	0.07	Buchhave_2016	Berger_2018	Gautier_2012
14	2.78578	0	6202	1.41	1.93	K-21 b	1	5.08	1.72	-1.72	1.639	0.019	-0.015	-0.1	Lopez-Morales_2016	Lopez-Morales_2016	Howell_2012
15	2.42629	0	5656	1.07	1.07	K-406 b	1	6.35	1.4	-1.4	1.558	0.148	-0.119	0.26	Marcy_2014	Berger_2018	Morton_2016
16	4.72674	0	5594	0.91	0.94	K-93 b	1	4.02	0.68	-0.68	1.642	0.069	-0.108	-0.2	Dressing_2015	Berger_2018	Ballard_2014
17	4.60358	0	4852	0.79	0.74	K-99 b	1	6.15	1.3	-1.3	1.511	0.073	-0.069	0.18	Marcy_2014	Berger_2018	Morton_2016
18	24.7371	0	3216	0.179	0.2139	LHS 1140 b	1	6.98	0.98	-0.98	1.727	0.032	-0.032	-0.24	Ment_2018	Ment_2018	Dittmann_2017
19	0.78964	0	5576	1.11	1.16	WASP-47 e	1	6.83	0.66	-0.66	1.81	0.027	-0.027	0.36	Vanderburg_2017	Vanderburg_2017	Almenara_2016
20	3.50473	1	5441	0.97	0.92	K-18 b	1	6.9	3.4	-3.4	1.765	0.185	-0.165	0.19	Cochran_2011	Berger_2018	Morton_2016

RV planets 2.0-3.0 Earth radii

1	41.6855	0	5766	1.67	1.08	K2-56 b	1	16.3	6	-6.1	2.6	0.1	-0.1	-0.15	Espinoza_2016	Stassun_2017	Mayo_2018
2	1.5804	0	3026	0.15	0.22	GJ 1214 b	1	6.26	0.86	-0.86	2.85	0.2	-0.2	0.15	Harpsoe_2013	Harpsoe_2013	Charbonneau_2009
3	9.4909	0	5175	0.75	0.74	HD 97658 b	1	7.86	0.73	-0.73	2.4	0.1	-0.1	-0.3	Dragomir_2013	Stassun_2017	Van_Grootel_2014
4	9.1205	0	5089	0.78	0.72	HIP 116454 b	1	11.82	1.33	-1.33	2.5	0.1	-0.1	-0.16	Vanderburg_2015	Stassun_2017	
5	10.0545	0	3896	0.6	0.56	K2-3 b	1	6.6	1.1	-1.1	2.29	0.23	-0.23	-0.01	Damasso_2018	Damasso_2018	Sinukoff_2016
6	13.8638	0	5010	0.74	0.71	K2-110 b	1	16.7	3.2	-3.2	2.6	0.1	-0.1	-0.34	Osborn_2017	Osborn_2017	Mayo_2018
7	32.9396	0	3457	0.36	0.41	K2-18 b	1	7.96	1.91	-1.91	2.38	0.22	-0.22	0.123	Cloutier_2017	Cloutier_2017	Benneke_2017
8	45.2943	1	5599	0.91	1.09	K-10 c	1	17.2	1.9	-1.9	2.35	0.1	-0.1	-0.15	Dumusque_2014	Berger_2018	Weiss_2016
9	16.1457	0	4909	0.81	0.73	K-102 e	1	8.93	2	-2	2.43	0.1	-0.2	0.18	Marcy_2014	Berger_2018	Morton_2016
10	13.5708	0	5860	1	1.04	K-106 c	1	10.44	3.2	-3.2	2.5	0.32	-0.32	-0.12	Marcy_2014	Marcy_2014	Morton_2016
11	43.8444	0	5860	1	1.04	K-106 e	1	11.17	5.8	-5.8	2.56	0.33	-0.33	-0.12	Marcy_2014	Marcy_2014	Morton_2016
12	16.092	0	5787	1.02	1	K-131 b	1	16.13	3.5	-3.5	2.4	0.2	-0.2	0.12	Marcy_2014	Marcy_2014	Morton_2016
13	9.287	0	5520	0.936	0.88	K-19 b	1	8.4	1.6	-1.5	2.3	0.1	-0.1	-0.08	Malavolta_2017	Berger_2018	Ballard_2011
14	77.6113	0	5508	0.95	0.89	K-20 d	1	10.07	3.97	-3.7	2.5	0.1	-0.1	0.07	Buchhave_2016	Berger_2018	Gautier_2012
15	6.2385	1	6285	1.19	1.36	K-25 b	1	9.6	4.2	-4.2	2.73	0.12	-0.11	-0.04	Marcy_2014	Berger_2018	Hadden_2014
16	10.5738	0	5678	1.03	1.08	K-454 b	1	6.84	1.4	-1.4	2.06	0.1	-0.2	0.27	Gettel_2016	Berger_2018	Stassun_2017
17	9.67395	1	5235	0.88	0.85	K-48 c	1	14.61	2.3	-2.3	2.56	0.1	-0.1	0.17	Marcy_2014	Berger_2018	Hadden_2014
18	5.39875	0	5789	1.08	1.26	K-68 b	1	8.3	2.2	-2.4	2.32	0.1	-0.1	0.12	Gilliland_2013	Berger_2018	van_Eylen_2015
19	16.2385	0	5751	1	0.95	K-96 b	1	8.46	3.4	-3.4	2.64	0.1	-0.24	0.04	Marcy_2014	Berger_2018	Morton_2016
20	4.754	0	4791	0.75	0.75	K-113 b	1	11.7	4.2	-4.2	2.16	0.1	-0.2	0.05	Marcy_2014	Berger_2018	Morton_2016
21	10.8541	0	5508	0.95	0.89	K-20 c	1	12.75	2.17	-2.24	2.87	0.19	-0.13	0.07	Buchhave_2016	Berger_2018	Gautier_2012

22	3.47175	0	4975	0.83	0.787	EPIC246471491 b	1	9.68	1.21	-1.37	2.59	0.06	-0.06	0.0	Palle_2018	Palle_2018	
23	50.81895	0	5372	0.88	0.85	K2-263 b	1	14.8	3.1	-3.1	2.41	0.12	-0.12	-0.08	Mortier_2018	Mortier_2018	
24	6.2682	0	6037	1.094	1.10	π Mensae c	1	4.82	0.84	-0.86	2.14	0.044	-0.044	0.08	Huang_2018	Huang_2018	Gandolfi_2018
RV planets 3.0-4.0 Earth radii																	
1	29.8454	0	5261	0.86	0.86	HD 3167 c	1	9.8	1.3	-1.24	3.01	0.42	-0.28	0.04	Christiansen_2017	Christiansen_2017	
2	10.9542	1	5466	0.956	0.906	K-88 b	1	8.7	2.5	-2.5	3.82	0.17	-0.34	0.2	Nesvorny_2013	Berger_2018	
3	2.50806	0	4728	0.81	0.747	K-94 b	1	10.84	1.4	-1.4	3.19	0.14	-0.25	0.34	Marcy_2018	Berger_2018	
4	11.5231	0	5654	1.08	1.418	K-95 b	1	13	2.9	-2.9	3.14	0.14	-0.13	0.3	Marcy_2018	Berger_2018	
5	7.138048	0	4975	0.83	0.787	EPIC246471491 c	1	15.68	2.28	-2.13	3.53	0.08	-0.08	0.0	Palle_2018	Palle_2018	
6	1.33735	0	5143	0.75	0.84	NGTS-4 b	1	20.6	3.0	-3.0	3.18	0.26	-0.26	-0.28	West_2018	West_2018	
RV planets 4.0-8.0 Earth radii																	
1	3.33665	0	3600	0.51	0.547	GJ 3470 b	1	13.9	1.5	-1.5	4.57	0.18	-0.18	0.18	Awlphan_2016	Awlphan_2016	
2	2.8492725	0	4300	0.688	0.715	K2-55 b	1	43.13	5.98	-5.8	4.41	0.32	-0.28	0.376	Dressing_2018	Dressing_2018	
3	3.185315	0	4985	0.85	0.81	HATS-7 b	1	38.1396	3.81396	-3.81396	6.311	0.516	-0.381	0.25	Bakos_2015	Bakos_2015	
4	11.81399	0	5499	1.12	1.66	HD 89345 b	1	35.7	3.3	-3.3	6.86	0.14	-0.14	0.45	Van_Eylen_2018	Van_Eylen_2018	
5	4.73401	0	5474	1.12	1.75	K2-108 b	1	59.4	4.4	-4.4	5.28	0.54	-0.54	0.33	Petigura_2017	Petigura_2017	Mayo_2018
6	8.99213	0	5275	0.86	0.84	K2-32 b	1	16.5	2.7	-2.7	5.13	0.28	-0.28	-0.02	Petigura_2017	Petigura_2017	Dai_2016
7	10.13675	0	6120	1.07	1.31	K2-98 b	1	32.2	8.1	-8.1	4.3	0.3	-0.2	-0.2	Barragan_2016	Barragan_2016	Mayo_2018
8	3.836169	0	4910	0.84	0.76	WASP-156 b	1	40.68224	3.1783	-2.86047	5.717	0.224	-0.224	0.24	Demangeon_2017	Demangeon_2017	
9	4.88782	0	4708	0.88	0.77	HAT-P-11 b	1	23.4	1.5	-1.5	4.36	0.06	-0.06	0.31	Yee_2018	Yee_2018	Bakos_2010
10	3.21346	0	5857	1.22	1.49	K-4 b	1	24.472	3.814	-3.814	4.076	0.181	-0.17	0.17	Borucki_2010	Berger_2018	Southworth_2011
11	6.21229	0	5080	0.88	0.77	CoRoT-8 b	1	69.92	9.53	-9.53	6.39	0.22	-0.22	0.3	Borde_2010	Borde_2010	Southworth_2011

12	4.23452	0	5079	1.12	0.87	HAT-P-26 b	1	22.2481	6.3566	-6.3566	7.062	0.448	-0.448	-0.04	Stassun_2017	Stassun_2017	Stevenson_2016
13	7.64159	1	5441	0.97	0.916	K-18 c	1	17.3	1.9	-1.9	4.263	0.183	-0.172	0.19	Cochran_2011	Berger_2018	Hadden_2014
14	14.85888	1	5441	0.97	0.916	K-18 d	1	16.4	1.4	-1.4	5.16	0.219	-0.215	0.19	Cochran_2011	Berger_2018	Hadden_Lithwich_2017
15	12.7204	1	6285	1.19	1.36	K-25 c	1	24.6	5.7	-5.7	5.134	0.216	-0.414	-0.04	Marcy_2014	Berger_2018	Hadden_2014
16	2.64388312	0	3416	0.47	0.455	GJ 436 b	1	21.36	0.2	-0.2	4.191	0.109	-0.109	0.02	Trifonov_2018	Turner_2016	Dressing_2018 Maciejewski_2014
TTV planets <8.0 Earth radii																	
1	10.3039	1	5763	1.04	1.091	K-11 b	0	2.78	0.64	-0.66	1.916	0.095	-0.081	-0.041	Bedell_2017	Berger_2018	
2	13.0241	1	5763	1.04	1.091	K-11 c	0	5	1.3	-1.35	3.006	0.138	-0.124	-0.041	Bedell_2017	Berger_2018	
3	22.6845	1	5763	1.04	1.091	K-11 d	0	8.13	0.67	-0.66	3.338	0.158	-0.138	-0.041	Bedell_2017	Berger_2018	
4	31.9996	1	5763	1.04	1.091	K-11 e	0	9.48	0.86	-0.88	4.3	0.188	-0.309	-0.041	Bedell_2017	Berger_2018	
5	46.6888	1	5836	1.04	1.091	K-11 f	0	2.53	0.49	-0.45	2.627	0.124	-0.116	-0.041	Bedell_2017	Berger_2018	
6	12.28	1	3884	0.54	0.607	K-26 b	0	5.12	0.65	-0.61	3.197	0.097	-0.093	-0.13	Jontof_Hutter_2016	Berger_2018	
7	17.2559	1	3884	0.54	0.607	K-26 c	0	6.2	0.65	-0.65	2.982	0.278	-0.229	-0.13	Jontof_Hutter_2016	Berger_2018	
8	10.3384	1	5378	0.98	0.749	K-29 b	0	4.51	1.41	-1.47	2.564	0.16	-0.141	-0.04	Jontof_Hutter_2016	Berger_2018	
9	13.2884	1	5378	0.98	0.749	K-29 c	0	4	1.23	-1.29	2.396	0.151	-0.133	-0.04	Jontof_Hutter_2016	Berger_2018	
10	29.33434	1	5454	0.99	0.834	K-30 b	0	8.8	0.6	-0.5	1.837	0.124	-0.171	0.18	Hadden_Lithwick_2017	Berger_2018	
11	13.83989	1	5979	1.07	1.652	K-36 b	0	3.9	0.2	-0.22	1.514	0.082	-0.071	-0.2	Hadden_Lithwick_2017	Berger_2018	
12	16.23855	1	5979	1.07	1.652	K-36 c	0	7.5	0.3	-0.3	3.688	0.165	-0.153	-0.2	Hadden_Lithwick_2017	Berger_2018	
13	45.154	1	5674	1.04	0.833	K-51 b	0	2.3	1.7	-1.6	6.559	0.316	-0.297	null	Hadden_Lithwick_2017	Berger_2018	

14	7.1334	1	5834	1.041	1.469	K-60 b	0	3.7	0.6	-0.6	1.845	0.339	-0.117	-0.09	Hadden_Lithwick_2017	Berger_2018	
15	8.9187	1	5834	1.041	1.469	K-60 c	0	2	0.3	-0.5	2.062	0.378	-0.131	-0.09	Hadden_Lithwick_2017	Berger_2018	
16	11.8981	1	5834	1.041	1.469	K-60 d	0	3.9	0.7	-0.6	1.901	0.495	-0.17	-0.09	Hadden_Lithwick_2017	Berger_2018	
17	27.4029	1	6389	1.17	1.345	K-79 c	0	5.9	1.9	-2.3	3.684	0.181	-0.165	-0.073	Jontof_Hutter_2014	Berger_2018	
18	52.0902	1	6389	1.17	1.345	K-79 d	0	6	2.1	-1.6	7.251	0.34	-0.322	-0.073	Jontof_Hutter_2014	Berger_2018	
19	81.0659	1	6389	1.17	1.345	K-79 e	0	4.1	1.2	-1.1	3.054	0.76	-0.186	-0.073	Jontof_Hutter_2014	Berger_2018	
20	7.05246	1	4665	0.73	0.681	K-80 b	0	6.93	1.05	-0.7	2.592	0.116	-0.11	0.04	MacDonald_2016	Berger_2018	
21	9.52355	1	4665	0.73	0.681	K-80 c	0	6.74	1.23	-0.86	2.594	0.121	-0.109	0.04	MacDonald_2016	Berger_2018	
22	3.07222	1	4665	0.73	0.681	K-80 d	0	6.75	0.69	-0.51	1.561	0.081	-0.064	0.04	MacDonald_2016	Berger_2018	
23	4.64489	1	4665	0.73	0.681	K-80 e	0	4.13	0.81	-0.95	1.602	0.081	-0.069	0.04	MacDonald_2016	Berger_2018	
24	10.4208	1	5559	0.91	0.936	K-307 b	0	8.8	0.9	-0.9	2.85	0.274	-0.208	0.19	Hadden_Lithwick_2017	Berger_2018	
25	13.0729	1	5559	0.91	0.936	K-307 c	0	3.9	0.7	-0.7	2.569	0.279	-0.211	0.19	Hadden_Lithwick_2017	Berger_2018	
26	66.0634	1	5989	1.08	1.013	K-289 d	0	4	0.9	-0.9	2.668	0.17	-0.17	0.05	Rowe_2014	Rowe_2014	
27	1.51087081	1	2559	0.08	0.12	TRAPPIST-1 b	0	1.22	0.15	-0.15	1.121	0.031	-0.032	0.04	Demory_2018	Grimm_2018	Delrez_2018
28	2.4218233	1	2559	0.08	0.12	TRAPPIST-1 c	0	1.24	0.15	-0.15	1.095	0.03	-0.031	0.04	Demory_2018	Grimm_2018	Delrez_2018
29	4.04961	1	2559	0.08	0.12	TRAPPIST-1 d	0	0.37	0.04	-0.04	0.784	0.023	-0.023	0.04	Demory_2018	Grimm_2018	Delrez_2018
30	6.099615	1	2559	0.08	0.12	TRAPPIST-1 e	0	0.66	0.079	-0.075	0.91	0.026	-0.027	0.04	Demory_2018	Grimm_2018	Delrez_2018
31	9.20669	1	2559	0.08	0.12	TRAPPIST-1 f	0	0.97	0.08	-0.078	1.046	0.029	-0.03	0.04	Demory_2018	Grimm_2018	Delrez_2018
32	12.35294	1	2559	0.08	0.12	TRAPPIST-1 g	0	1.27	0.098	-0.095	1.148	0.032	-0.033	0.04	Demory_2018	Grimm_2018	Delrez_2018
33	18.767	1	2559	0.08	0.12	TRAPPIST-1 h	0	0.37	0.049	-0.056	0.773	0.027	-0.026	0.04	Demory_2018	Grimm_2018	Delrez_2018

References for SI reference citations

1. R. L. Akeson *et al.*, The NASA Exoplanet Archive: Data and Tools for Exoplanet Research. *Publ. Astron. Soc. Pacific*. **125**, 989 (2013).
2. S. E. Thompson *et al.*, Planetary Candidates Observed by Kepler. VIII. A Fully Automated Catalog With Measured Completeness and Reliability Based on Data Release 25. *Astrophys. J. Suppl. Ser. Vol. 235, Issue 2, Artic. id. 38, 49 pp. (2018)*. **235** (2017), doi:10.3847/1538-4365/aab4f9.
3. K. G. Stassun, E. Corsaro, J. A. Pepper, B. S. Gaudi, Empirical Accurate Masses and Radii of Single Stars with *TESS* and *Gaia*. *Astron. J.* **155**, 22 (2017).
4. T. A. Berger, D. Huber, E. Gaidos, J. L. van Saders, Revised Radii of Kepler Stars and Planets using Gaia Data Release 2 (2018) (available at http://arxiv.org/abs/1805.00231).
5. C. M. Persson *et al.*, An 8 Mearth super-Earth in a 2.2 day orbit around the K5V star K2-216 (2018) (available at http://arxiv.org/abs/1805.04774).
6. A. W. Mayo *et al.*, 275 Candidates and 149 Validated Planets Orbiting Bright Stars in K2 Campaigns 0-10. *Astron. Journal, Vol. 155, Issue 3, Artic. id. 136, 25 pp. (2018)*. **155** (2018), doi:10.3847/1538-3881/aaadff.
7. B. O. Demory *et al.*, A map of the large day-night temperature gradient of a super-Earth exoplanet. *Nature*. **532** (2016), doi:10.1038/nature17169.
8. J. ~N. Winn *et al.*, A Super-Earth Transiting a Naked-eye Star. *\apjl*. **737**, L18 (2011).
9. S. ~C. ~C. Barros *et al.*, Revisiting the transits of CoRoT-7b at a lower activity level. *\aap*. **569**, A74 (2014).
10. R. ~D. Haywood *et al.*, Planets and stellar activity: hide and seek in the CoRoT-7 system. *\mnras*. **443**, 2517–2531 (2014).
11. M. Gillon *et al.*, Two massive rocky planets transiting a K-dwarf 6.5 parsecs away (2017), doi:10.1038/s41550-017-0056.
12. F. Motalebi *et al.*, The HARPS-N Rocky Planet Search I. HD219134b: A transiting rocky planet in a multi-planet system at 6.5 pc from the Sun. *Astron. Astrophys. Vol. 584, id.A72, 12 pp.* **584** (2015), doi:10.1051/0004-6361/201526822.
13. J. L. Christiansen *et al.*, Three's Company: An Additional Non-transiting Super-Earth in the Bright HD 3167 System, and Masses for All Three Planets. *Astron. J.* **154**, 122 (2017).
14. D. Gandolfi *et al.*, The Transiting Multi-planet System HD 3167: A 5.7 $M_{\oplus}$ Super-Earth and an 8.3 $M_{\oplus}$ Mini-Neptune. *Astron. J.* **154**, 123 (2017).
15. M. Damasso *et al.*, Eyes on K2-3: A system of three likely sub-Neptunes characterized with HARPS-N and HARPS (2018) (available at http://arxiv.org/abs/1802.08320).
16. E. Sinukoff *et al.*, Eleven Multi-planet Systems from K2 Campaigns 1 & 2 and the Masses of Two Hot Super-Earths. *Astrophys. Journal, Vol. 827, Issue 1, Artic. id. 78, 27 pp. (2016)*. **827** (2015), doi:10.3847/0004-637X/827/1/78.
17. E. W. Guenther *et al.*, K2-106, a system containing a metal-rich planet and a planet of lower density (2017), doi:10.1051/0004-6361/201730885.
18. E. R. Adams *et al.*, Ultra Short Period Planets in K2 with companions: a double transiting system for EPIC 220674823. *Astron. Journal, Vol. 153, Issue 2, Artic. id. 82, 7 pp. (2017)*. **153** (2016), doi:10.3847/1538-3881/153/2/82.
19. E. Sinukoff *et al.*, K2-66b and K2-106b: Two extremely hot sub-Neptune-size planets with high densities. *Astron. Journal, Vol. 153, Issue 6, Artic. id. 271, 13 pp. (2017)*. **153** (2017), doi:10.3847/1538-3881/aa725f.
20. F. Dai *et al.*, The Discovery and Mass Measurement of a New Ultra-short-period Planet:

K2-131b. *Astron. J.* **154**, 226 (2017).
21. L. Malavolta *et al.*, An ultra-short period rocky super-Earth with a secondary eclipse and a Neptune-like companion around K2-141 (2018), doi:10.3847/1538-3881/aaa5b5.
22. O. Barragán *et al.*, K2-141 b: A 5-M$_\oplus$ super-Earth transiting a K7 V star every 6.7 hours. *Astron. Astrophys. Vol. 612, id.A95, 11 pp.* **612** (2017), doi:10.1051/0004-6361/201732217.
23. L. ~J. Esteves, E. ~J. ~W. De Mooij, R. Jayawardhana, Changing Phases of Alien Worlds: Probing Atmospheres of Kepler Planets with High-precision Photometry. *\apj*. **804**, 150 (2015).
24. X. Dumusque *et al.*, The Kepler-10 Planetary System Revisited by HARPS-N: A Hot Rocky World and a Solid Neptune-Mass Planet. *\apj*. **789**, 154 (2014).
25. G. W. Marcy *et al.*, Masses, Radii, and Orbits of Small Kepler Planets: The Transition from Gaseous to Rocky Planets. **20** (2014), doi:10.1088/0067-0049/210/2/20.
26. L. A. Buchhave *et al.*, A 1.9 Earth radius rocky planet and the discovery of a non-transiting planet in the Kepler-20 system. *Astron. Journal, Vol. 152, Issue 6, Artic. id. 160, 12 pp. (2016).* **152** (2016), doi:10.3847/0004-6256/152/6/160.
27. T. N. Gautier *et al.*, Kepler-20: A Sun-like Star with Three Sub-Neptune Exoplanets and Two Earth-size Candidates. *Astrophys. J.* **749**, 15 (2012).
28. M. Lopez-Morales *et al.*, Kepler-21b: A rocky planet around a V = 8.25 magnitude star. *ArXiv e-prints* (2016).
29. S. B. Howell *et al.*, Kepler-21b: A 1.6 R Earth Planet Transiting the Bright Oscillating F Subgiant Star HD 179070. *Astrophys. J.* **746**, 123 (2012).
30. T. D. Morton *et al.*, False positive probabilties for all Kepler Objects of Interest: 1284 newly validated planets and 428 likely false positives. *Astrophys. Journal, Vol. 822, Issue 2, Artic. id. 86, 15 pp. (2016).* **822** (2016), doi:10.3847/0004-637X/822/2/86.
31. C. ~D. Dressing *et al.*, The Mass of Kepler-93b and The Composition of Terrestrial Planets. *\apj*. **800**, 135 (2015).
32. S. Ballard *et al.*, Kepler-93b: A Terrestrial World Measured to within 120 km, and a Test Case for a New Spitzer Observing Mode. *Astrophys. J.* **790**, 12 (2014).
33. W. J. Borucki *et al.*, Kepler-22b: A 2.4 Earth-radius Planet in the Habitable Zone of a Sun-like Star. *Astrophys. J.* **745**, 120 (2012).
34. J. A. Dittmann *et al.*, A temperate rocky super-Earth transiting a nearby cool star. *Nature, Vol. 544, Issue 7650, pp. 333-336 (2017).* **544**, 333–336 (2017).
35. A. Vanderburg *et al.*, Precise Masses in the WASP-47 System (2017), doi:10.3847/1538-3881/aa918b.
36. J. M. Almenara, R. F. Díaz, X. Bonfils, S. Udry, Absolute densities, masses, and radii of the WASP-47 system determined dynamically. *Astron. Astrophys. Vol. 595, id.L5, 12 pp.* **595** (2016), doi:10.1051/0004-6361/201629770.
37. X. Bonfils *et al.*, Radial velocity follow-up of GJ1132 with HARPS. A precise mass for planet "b" and the discovery of a second planet (2018) (available at http://arxiv.org/abs/1806.03870).
38. N. Espinoza *et al.*, Discovery and Validation of a High-Density sub-Neptune from the K2 Mission. *Astrophys. Journal, Vol. 830, Issue 1, Artic. id. 43, 11 pp. (2016).* **830** (2016), doi:10.3847/0004-637X/830/1/43.
39. K. B. W. Harpsøe *et al.*, The Transiting System GJ1214: High-Precision Defocused Transit Observations and a Search for Evidence of Transit Timing Variation. *Astron.*

Astrophys. Vol. 549, id.A10, 10 pp. **549** (2012), doi:10.1051/0004-6361/201219996.
40. D. Charbonneau *et al.*, A super-Earth transiting a nearby low-mass star. *\nat*. **462**, 891–894 (2009).
41. D. Dragomir *et al.*, MOST Detects Transits of HD 97658b, a Warm, Likely Volatile-rich Super-Earth. *\apjl*. **772**, L2 (2013).
42. V. Van Grootel *et al.*, Transit confirmation and improved stellar and planet parameters for the super-Earth HD 97658 b and its host star. *Astrophys. Journal, Vol. 786, Issue 1, Artic. id. 2, 11 pp. (2014).* **786** (2014), doi:10.1088/0004-637X/786/1/2.
43. A. Vanderburg *et al.*, Characterizing K2 Planet Discoveries: A Super-Earth Transiting the Bright K Dwarf HIP{\nbsp}116454. *\apj*. **800**, 59 (2015).
44. H. P. Osborn *et al.*, K2-110 b - a massive mini-Neptune exoplanet. *Astron. Astrophys. Vol. 604, id.A19, 8 pp.* **604** (2016), doi:10.1051/0004-6361/201628932.
45. R. Cloutier *et al.*, Characterization of the K2-18 multi-planetary system with HARPS: A habitable zone super-Earth and discovery of a second, warm super-Earth on a non-coplanar orbit. *Astron. Astrophys. Vol. 608, id.A35, 13 pp.* **608** (2017), doi:10.1051/0004-6361/201731558.
46. B. Benneke *et al.*, Spitzer Observations Confirm and Rescue the Habitable-Zone Super-Earth K2-18b for Future Characterization. *Astrophys. Journal, Vol. 834, Issue 2, Artic. id. 187, 10 pp. (2017).* **834** (2016), doi:10.3847/1538-4357/834/2/187.
47. L. M. Weiss *et al.*, Revised Masses and Densities of the Planets around Kepler-10. *Astrophys. Journal, Vol. 819, Issue 1, Artic. id. 83, 22 pp. (2016).* **819** (2016), doi:10.3847/0004-637X/819/1/83.
48. L. Malavolta *et al.*, The Kepler-19 System: A Thick-envelope Super-Earth with Two Neptune-mass Companions Characterized Using Radial Velocities and Transit Timing Variations. *Astron. Journal, Vol. 153, Issue 5, Artic. id. 224, 14 pp. (2017).* **153** (2017), doi:10.3847/1538-3881/aa6897.
49. S. Ballard *et al.*, The Kepler-19 System: A Transiting 2.2 R ⊕ Planet and a Second Planet Detected via Transit Timing Variations. *Astrophys. Journal, Vol. 743, Issue 2, Artic. id. 200, 20 pp. (2011).* **743** (2011), doi:10.1088/0004-637x/743/2/200.
50. S. Hadden, Y. Lithwick, Densities and Eccentricities of 139 Kepler Planets from Transit Time Variations. *Astrophys. Journal, Vol. 787, Issue 1, Artic. id. 80, 7 pp. (2014).* **787** (2014), doi:10.1088/0004-637x/787/1/80.
51. S. Gettel *et al.*, The Kepler-454 System: A Small, Not-rocky Inner Planet, a Jovian World, and a Distant Companion. *Astrophys. Journal, Vol. 816, Issue 2, Artic. id. 95, 13 pp. (2016).* **816** (2015), doi:10.3847/0004-637X/816/2/95.
52. R. L. Gilliland *et al.*, Kepler-68: Three Planets, One with a Density between that of Earth and Ice Giants. *Astrophys. J.* **766**, 40 (2013).
53. V. Van Eylen, S. Albrecht, Eccentricity from transit photometry: small planets in Kepler multi-planet systems have low eccentricities. *Astrophys. Journal, Vol. 808, Issue 2, Artic. id. 126, 20 pp. (2015).* **808** (2015), doi:10.1088/0004-637X/808/2/126.
54. G. Á. Bakos *et al.*, HATS-7b: A Hot Super Neptune Transiting a Quiet K Dwarf Star. *Astrophys. Journal, Vol. 813, Issue 2, Artic. id. 111, 10 pp. (2015).* **813** (2015), doi:10.1088/0004-637X/813/2/111.
55. S. W. Yee *et al.*, HAT-P-11: Discovery of a Second Planet and a Clue to Understanding Exoplanet Obliquities. *Astron. Journal, Vol. 155, Issue 6, Artic. id. 255, 13 pp. (2018).* **155** (2018), doi:10.3847/1538-3881/aabfec.

56. V. Van Eylen *et al.*, HD 89345: a bright oscillating star hosting a transiting warm Saturn-sized planet observed by K2. *Mon. Not. R. Astron. Soc. Vol. 478, Issue 4, p.4866-4880.* **478**, 4866–4880 (2018).
57. E. A. Petigura *et al.*, Four Sub-Saturns with Dissimilar Densities: Windows into Planetary Cores and Envelopes. *Astron. Journal, Vol. 153, Issue 4, Artic. id. 142, 19 pp. (2017).* **153** (2017), doi:10.3847/1538-3881/aa5ea5.
58. F. Dai *et al.*, Doppler Monitoring of five K2 Transiting Planetary Systems. *Astrophys. Journal, Vol. 823, Issue 2, Artic. id. 115, 16 pp. (2016).* **823** (2016), doi:10.3847/0004-637X/823/2/115.
59. O. Barragán *et al.*, K2-98 b: A 32-M$_\oplus$ Neptune-sized planet in a 10-day orbit transiting an F8 star. *Astron. Journal, Vol. 152, Issue 6, Artic. id. 193, 9 pp. (2016).* **152** (2016), doi:10.3847/0004-6256/152/6/193.
60. O. D. S. Demangeon *et al.*, The discovery of WASP-151b, WASP-153b, WASP-156b: Insights on giant planet migration and the upper boundary of the Neptunian desert. *Astron. Astrophys. Vol. 610, id.A63, 19 pp.* **610** (2017), doi:10.1051/0004-6361/201731735.
61. P. Bordé *et al.*, Transiting exoplanets from the CoRoT space mission. XI. CoRoT-8b: a hot and dense sub-Saturn around a K1 dwarf. *Astron. Astrophys. Vol. 520, id.A66, 10 pp.* **520** (2010), doi:10.1051/0004-6361/201014775.
62. J. Southworth, John, Homogeneous studies of transiting extrasolar planets. IV. Thirty systems with space-based light curves. *Mon. Not. R. Astron. Soc. Vol. 417, Issue 3, pp. 2166-2196.* **417**, 2166–2196 (2011).
63. K. B. Stevenson *et al.*, A Search for Water in the Atmosphere of HAT-P-26b Using LDSS-3C. *Astrophys. Journal, Vol. 817, Issue 2, Artic. id. 141, 10 pp. (2016).* **817** (2015), doi:10.3847/0004-637X/817/2/141.
64. T. Trifonov *et al.*, The CARMENES search for exoplanets around M dwarfs. First visual-channel radial-velocity measurements and orbital parameter updates of seven M-dwarf planetary systems. *Astron. Astrophys. Vol. 609, id.A117, 24 pp.* **609** (2017), doi:10.1051/0004-6361/201731442.
65. J. D. Turner *et al.*, Ground-based near-UV observations of 15 transiting exoplanets: Constraints on their atmospheres and no evidence for asymmetrical transits. *Mon. Not. R. Astron. Soc. Vol. 459, Issue 1, p.789-819*. **459**, 789–819 (2016).
66. G. Maciejewski *et al.*, On the GJ 436 planetary system. *Acta Astron. vol 64, no 4, p. 323-335*. **64**, 323–335 (2015).
67. T. Holczer *et al.*, Transit Timing Observations from Kepler. IX. Catalog of the Full Long-cadence Data Set. *apjs*. **225**, 9 (2016).
68. D. Jontof-Hutter *et al.*, Secure Mass Measurements from Transit Timing: 10 Kepler Exoplanets between 3 and 8 M⊕ with Diverse Densities and Incident Fluxes. *Astrophys. J.* **820**, 39 (2016).
69. S. Hadden, Y. Lithwick, Kepler Planet Masses and Eccentricities from Transit Timing Variations. *Am. Astron. Soc. AAS Meet. #229, id.401.03*. **229** (2017) (available at http://adsabs.harvard.edu/abs/2017AAS...22940103H).
70. S. L. Grimm *et al.*, The nature of the TRAPPIST-1 exoplanets (2018), doi:10.1051/0004-6361/201732233.
71. J. J. Lissauer *et al.*, A closely packed system of low-mass, low-density planets transiting Kepler-11. *Nature*. **470**, 53–58 (2011).
72. M. Bedell *et al.*, Kepler-11 is a Solar Twin: Revising the Masses and Radii of Benchmark

Planets via Precise Stellar Characterization. *Astrophys. J.* **839**, 94 (2017).
73. J. A. Carter *et al.*, Kepler-36: A Pair of Planets with Neighboring Orbits and Dissimilar Densities. *Science (80-.).* **337**, 556–559 (2012).
74. K. Ment *et al.*, A second planet with an Earth-like composition orbiting the nearby M dwarf LHS 1140 (2018) (available at http://arxiv.org/abs/1808.00485).
75. E. Palle *et al.*, Detection and Doppler monitoring of EPIC 246471491, a system of four transiting planets smaller than Neptune (2018) (available at https://arxiv.org/abs/1808.00575).
76. L. Delrez *et al.*, Early 2017 observations of TRAPPIST-1 with Spitzer. *Mon. Not. R. Astron. Soc.* **475**, 3577–3597 (2018).
77. A. Mortier *et al.*, K2-263 b: a 50 d period sub-Neptune with a mass measurement using HARPS-N. *Mon. Not. R. Astron. Soc. Vol. 481, Issue 2, p.1839-1847.* **481**, 1839–1847 (2018).
78. C. X. Huang *et al.*, TESS Discovery of a Transiting Super-Earth in the Π Mensae System (2018) (available at http://arxiv.org/abs/1809.05967).
79. D. Gandolfi *et al.*, TESS's first planet: a super-Earth transiting the naked-eye star π Mensae (2018) (available at http://arxiv.org/abs/1809.07573).
80. R. G. West *et al.*, NGTS-4b: A sub-Neptune Transiting in the Desert (2018) (available at http://arxiv.org/abs/1809.00678).
81. J. N. Winn, in *Handbook of Exoplanets*, H. J. Deeg, J. . Belmonte, Eds. (Springer, 2018; http://arxiv.org/abs/1801.08543).
82. C. W. Ormel, B. Liu, D. Schoonenberg, Formation of TRAPPIST-1 and other compact systems. *Astron. Astrophys.* **604**, A1 (2017).
83. M. Gillon *et al.*, Seven temperate terrestrial planets around the nearby ultracool dwarf star TRAPPIST-1. *Nature*. **542**, 456–460 (2017).
84. F. Fressin *et al.*, Two Earth-sized planets orbiting Kepler-20. *\nat*. **482**, 195–198 (2012).
85. T. N. Gautier *et al.*, Kepler-20: A Sun-like Star with Three Sub-Neptune Exoplanets and Two Earth-size Candidates. *Astrophys. Journal, Vol. 749, Issue 1, Artic. id. 15, 19 pp. (2012).* **749** (2011), doi:10.1088/0004-637X/749/1/15.
86. A. S. Bonomo *et al.*, A giant impact as the likely origin of different twins in the Kepler-107 exoplanet system. *Nat. Astron.*, 1 (2019).
87. J. ~F. Rowe *et al.*, Validation of Kepler's Multiple Planet Candidates. III. Light Curve Analysis and Announcement of Hundreds of New Multi-planet Systems. *\apj*. **784**, 45 (2014).
88. S. Hadden, Y. Lithwick, Numerical and analytical modeling of transit timing variations. *ApJ*. **828**, 44 (2016).
89. S. Wang, D.-H. Wu, T. Barclay, G. P. Laughlin, Updated Masses for the TRAPPIST-1 Planets (2017) (available at http://arxiv.org/abs/1704.04290).
90. C. T. Unterborn, S. J. Desch, N. R. Hinkel, A. Lorenzo, Inward migration of the TRAPPIST-1 planets as inferred from their water-rich compositions. *Nat. Astron.* **2**, 297–302 (2018).
91. T. D. Morton, J. N. Winn, Obliquities of kepler stars: comparison of single- and multiple-transit systems. *Astrophys. J.* **796**, 47 (2014).
92. J. M. Brewer, S. Wang, D. A. Fischer, D. Foreman-Mackey, Compact Multi-planet Systems are more Common around Metal-poor Hosts. *Astrophys. J.* **867**, L3 (2018).
93. R. I. Dawson, E. J. Lee, E. Chiang, Correlations Between Compositions and Orbits

Established By the Giant Impact Era of Planet Formation. *Astrophys. J.* **822**, 54 (2016).
94. J. Moriarty, S. Ballard, The kepler dichotomy in planetary disks: linking kepler observables to simulations of late-stage planet formation. *Astrophys. J.* **832** (2016), doi:10.3847/0004-637X/832/1/34.
95. C. D. Dressing *et al.*, Characterizing K2 Candidate Planetary Systems Orbiting Low-Mass Stars III: A High Mass & Low Envelope Fraction for the Warm Neptune K2-55b (2018) (available at http://arxiv.org/abs/1804.05148).
96. H. Mizuno, Formation of the Giant Planets. *Prog. Theor. Phys.* **64**, 544–557 (1980).
97. D. J. Stevenson, Formation of the giant planets. *Planet. Space Sci.* **30**, 755–764 (1982).
98. A.-M. A. Piso, A. N. Youdin, on the minimum core mass for giant planet formation at wide separations. *Astrophys. J.* **786**, 21 (2014).
99. S. L. Li, C. B. Agnor, D. N. C. Lin, Embryo impacts and gas giant mergers. I. dichotomy of jupiter and saturn's core mass. *Astrophys. J.* **720**, 1161–1173 (2010).
100. S.-F. Liu, C. B. Agnor, D. N. C. Lin, S.-L. Li, Embryo impacts and gas giant mergers – II. Diversity of hot Jupiters' internal structure. *Mon. Not. R. Astron. Soc.* **446**, 1685–1702 (2015).
101. A. Bhattacharya *et al.*, WFIRST Exoplanet Mass Measurement Method Finds a Planetary Mass of $39\pm 8 M_\oplus$ for OGLE-2012-BLG-0950Lb (2018) (available at https://arxiv.org/abs/1809.02654).
102. D. Suzuki *et al.*, The exoplanet mass-ratio function from the MOA-II survey: discovery of a break and likely peak at a Neptune mass. *Astrophys. J.* **833**, 145 (2016).
103. E. J. Lee, E. Chiang, Breeding super-earths and birthing super-puffs in transitional disks. *Astrophys. J.* **817**, 90 (2016).
104. M. Ansdell *et al.*, ALMA Survey of Lupus Protoplanetary Disks. I. Dust and Gas Masses. *Astrophys. Journal, Vol. 828, Issue 1, Artic. id. 46, 15 pp. (2016).* **828** (2016), doi:10.3847/0004-637x/828/1/46.
105. M. Ansdell *et al.*, ALMA Survey of Lupus Protoplanetary Disks. II. Gas Disk Radii. *Astrophys. J.* **859**, 21 (2018).
106. S. Seager, M. Kuchner, C. A. Hier-Majumder, B. Militzer, Mass-Radius Relationships for Solid Exoplanets. *Astrophys. J.* **669**, 1279–1297 (2007).
107. L. Zeng, S. Seager, A Computational Tool to Interpret the Bulk Composition of Solid Exoplanets based on Mass and Radius Measurements. *Publ. Astron. Soc. Pacific*. **120**, 983–991 (2008).
108. L. Zeng, D. D. Sasselov, S. B. Jacobsen, Mass-Radius Relation for Rocky Planets Based on PREM. *Astrophys. J.* **819**, 127 (2016).
109. L. Zeng, D. Sasselov, A Detailed Model Grid for Solid Planets from 0.1 through 100 Earth Masses. *Publ. Astron. Soc. Pacific*. **125**, 227–239 (2013).
110. D. C. Swift *et al.*, Mass-Radius Relationships for Exoplanets. *Astrophys. J.* **744**, 59 (2012).
111. R. F. Smith *et al.*, Equation of state of iron under core conditions of large rocky exoplanets. *Nat. Astron.* **2**, 452–458 (2018).
112. F. ~W. Wagner, F. Sohl, H. Hussmann, M. Grott, H. Rauer, Interior structure models of solid exoplanets using material laws in the infinite pressure limit. *Icarus*. **214**, 366–376 (2011).
113. F. ~W. Wagner, N. Tosi, F. Sohl, H. Rauer, T. Spohn, Rocky super-Earth interiors. Structure and internal dynamics of CoRoT-7b and Kepler-10b. *\aap*. **541**, A103 (2012).

114. D. Valencia, D. D. Sasselov, R. J. O'Connell, Detailed Models of Super-Earths: How Well Can We Infer Bulk Properties? *Astrophys. J.* **665**, 1413–1420 (2007).
115. Valencia, D., Ikoma, M., Guillot, T., Nettelmann, N., Composition and fate of short-period super-Earths. *A&A*. **516**, A20 (2010).
116. C. Sotin, O. Grasset, A. Mocquet, Mass-radius curve for extrasolar Earth-like planets and ocean planets. *Icarus*. **191**, 337–351 (2007).
117. O. Grasset, J. Schneider, C. Sotin, A Study of the Accuracy of Mass-Radius Relationships for Silicate-Rich and Ice-Rich Planets up to 100 Earth Masses. *Astrophys. J.* **693**, 722–733 (2009).
118. H. S. Zapolsky, E. E. Salpeter, The Mass-Radius Relation for Cold Spheres of Low Mass. *Astrophys. J.* **158**, 809 (1969).
119. J. J. Fortney, M. S. Marley, J. W. Barnes, Planetary Radii Across Five Orders of Magnitude in Mass and Stellar Insolation: Application to Transits. *Astrophys. J.* **659**, 1661–1672 (2007).
120. C. ~T. Unterborn, E. ~E. Dismukes, W. ~R. Panero, Scaling the Earth: A Sensitivity Analysis of Terrestrial Exoplanetary Interior Models. *ArXiv e-prints* (2015).
121. D. Saumon, G. Chabrier, H. M. van Horn, An Equation of State for Low-Mass Stars and Giant Planets. *Astrophys. J. Suppl. Ser.* **99**, 713 (1995).
122. A. Becker *et al.*, ab initio equations of state for hydrogen (H-REOS.3) and helium (He-REOS.3) and their implications for the interior of brown dwarfs. *Astrophys. J. Suppl. Ser.* **215**, 21 (2014).
123. B. Militzer, W. B. Hubbard, ab initio equation of state for hydrogen-helium mixtures with recalibration of the giant-planet mass-radius relation. *Astrophys. J.* **774**, 148 (2013).
124. M. Chaplin, Water Phase Diagram (2018).
125. M. R. Frank, Y. Fei, J. Hu, Constraining the equation of state of fluid H2O to 80 GPa using the melting curve, bulk modulus, and thermal expansivity of Ice VII. *Geochim. Cosmochim. Acta*. **68**, 2781–2790 (2004).
126. M. French, R. Redmer, Construction of a thermodynamic potential for the water ices VII and X. *Phys. Rev. B*. **91**, 14308 (2015).
127. M. French, T. R. Mattsson, N. Nettelmann, R. Redmer, Equation of state and phase diagram of water at ultrahigh pressures as in planetary interiors. *Phys. Rev. B*. **79**, 54107 (2009).
128. M. Millot *et al.*, Experimental evidence for superionic water ice using shock compression. *Nat. Phys.*, 1 (2018).
129. C. Cavazzoni *et al.*, Superionic and Metallic States of Water and Ammonia at Giant Planet Conditions. *Science (80-.).* **283**, 44 (1999).
130. J.-A. Hernandez, R. Caracas, Superionic-Superionic Phase Transitions in Body-Centered Cubic H 2 O Ice. *Phys. Rev. Lett.* **117**, 135503 (2016).
131. L. Zeng, D. D. Sasselov, The Effect of Temperature Evolution on the Interior Structure of H2O-rich Planets. *Astrophys. J.* **784**, 96 (2014).
132. "The International Association for the Properties of Water and Steam Revised Release on the IAPWS Formulationd 1995 for the Thermodynamic Properties of Ordinary Water Substance for General and Scientific Use" (2016), (available at http://www.iapws.org.).
133. R. B. Dooley, K. Daucik, "The International Association for the Properties of Water and Steam Revised Release on the Pressure along the Melting and Sublimation Curves of Ordinary Water Substance" (2011), (available at http://www.iapws.org.).

134. W. Wagner, T. Riethmann, R. Feistel, A. H. Harvey, New Equations for the Sublimation Pressure and Melting Pressure of H_2O Ice Ih. *J. Phys. Chem. Ref. Data*. **40**, 43103 (2011).
135. M. D. Knudson *et al.*, Probing the Interiors of the Ice Giants: Shock Compression of Water to 700 GPa and 3.8 g / cm^3. *Phys. Rev. Lett.* **108**, 91102 (2012).
136. E. Sugimura *et al.*, Experimental evidence of superionic conduction in H2O ice. *J. Chem. Phys.* **137** (2012), doi:10.1063/1.4766816.
137. R. Redmer, T. R. Mattsson, N. Nettelmann, M. French, The phase diagram of water and the magnetic fields of Uranus and Neptune. *Icarus*. **211**, 798–803 (2011).
138. E. R. Adams, S. Seager, L. Elkins-Tanton, Ocean Planet or Thick Atmosphere: On the Mass-Radius Relationship for Solid Exoplanets with Massive Atmospheres. *Astrophys. J.* **673**, 1160–1164 (2008).
139. E. D. Lopez, J. J. Fortney, Understanding the Mass-Radius Relation for Sub-neptunes: Radius as a Proxy for Composition. *ApJ.* **792**, 1 (2014).
140. D. Valencia, R. J. O'Connell, D. Sasselov, Internal structure of massive terrestrial planets. *Icarus*. **181**, 545–554 (2006).
141. D. D. Sasselov, M. Lecar, On the Snow Line in Dusty Protoplanetary Disks. *Astrophys. J.* **528**, 995 (2000).
142. T. Sato, S. Okuzumi, S. Ida, On the water delivery to terrestrial embryos by ice pebble accretion. *A&A*. **589** (2016), doi:10.1051/0004-6361/201527069.
143. R. G. Martin, M. Livio, On the evolution of the snow line in protoplanetary discs. *Mon. Not. R. Astron. Soc. Lett.* **425**, L6–L9 (2012).
144. W. Kley, R. P. Nelson, Planet-Disk Interaction and Orbital Evolution. *Annu. Rev. Astron. Astrophys.* **50**, 211–249 (2012).
145. P. J. Armitage, *Astrophysics of Planet Formation* (Cambridge University Press, 2010; http://adsabs.harvard.edu/abs/2010apf..book.....A).
146. S. N. Raymond, C. Cossou, No universal minimum-mass extrasolar nebula: evidence against in situ accretion of systems of hot super-Earths. *Mon. Not. R. Astron. Soc. Lett.* **440**, L11–L15 (2014).
147. S. N. Raymond *et al.*, Planet-planet scattering leads to tightly packed planetary systems. *Astrophys. J.* **696**, L98–L101 (2009).